

The host galaxy and *Fermi*-LAT counterpart of HESS J1943+213

D. Peter¹, W. Domainko², D. A. Sanchez³, A. van der Wel¹, and W. Gässler¹¹ Max-Planck-Institut für Astronomie, Königstuhl 17, 69117 Heidelberg, Germany
e-mail: peterd@mpia.de² Max-Planck-Institut für Kernphysik, Saupfercheckweg 1, 69117 Heidelberg, Germany³ Laboratoire d'Annecy-le-Vieux de Physique des Particules, Université de Savoie, CNRS/IN2P3, 74941 Annecy-le-Vieux, France

Received 14 March 2014 / Accepted 15 August 2014

ABSTRACT

Context. The very-high energy (VHE, $E > 100$ GeV) gamma-ray sky shows diverse Galactic and extragalactic source populations. For some sources the astrophysical object class could not be identified so far.

Aims. The nature (Galactic or extragalactic) of the VHE gamma-ray source HESS J1943+213 is explored. We specifically investigate the proposed near-infrared counterpart 2MASS J19435624+2118233 of HESS J1943+213 and investigate the implications of a physical association.

Methods. We present *K*-band imaging from the 3.5 m CAHA telescope of 2MASS J19435624+2118233. Furthermore, 5 years of *Fermi*-LAT data were analyzed to search for a high-energy (HE, $100 \text{ MeV} < E < 100 \text{ GeV}$) counterpart.

Results. The CAHA observations revealed that the near-infrared counterpart is extended with an intrinsic half light radius of $2''\text{--}2.5''$. These observations also show a smooth, centrally concentrated light profile that is typical of a galaxy, and thus point toward an extragalactic scenario for the VHE gamma-ray source, assuming that the near-infrared source is the counterpart of HESS J1943+213. A high-Sérsic index profile provides a better fit than an exponential profile, indicating that the surface brightness profile of 2MASS J19435624+2118233 follows that of a typical, massive elliptical galaxy more closely than that of a disk galaxy. With *Fermi*-LAT a HE counterpart is found with a power-law spectrum above 1 GeV, with a normalization of $(3.0 \pm 0.8_{\text{stat}} \pm 0.6_{\text{sys}}) \times 10^{-15} \text{ cm}^{-2} \text{ s}^{-1} \text{ MeV}^{-1}$ at the decorrelation energy $E_{\text{dec}} = 15.1 \text{ GeV}$ and a spectral index of $\Gamma = 1.59 \pm 0.19_{\text{stat}} \pm 0.13_{\text{sys}}$. This gamma-ray spectrum shows a rather sharp break between the HE and VHE regimes of $\Delta\Gamma = 1.47 \pm 0.36$.

Conclusions. The infrared and HE data strongly favor an extragalactic origin of HESS J1943+213, where the infrared counterpart traces the host galaxy of an extreme blazar and where the rather sharp spectral break between the HE and VHE regime indicates attenuation on extragalactic background light. The source is most likely located at a redshift between 0.03 and 0.45 according to extension and EBL attenuation arguments.

Key words. galaxies: elliptical and lenticular, cD – BL Lacertae objects: individual: HESS J1943+213 – gamma rays: galaxies – radiation mechanisms: non-thermal

1. Introduction

In recent years a variety of very-high energy (VHE, $E > 100$ GeV) gamma-ray sources of extragalactic and Galactic origin have been discovered. It has been found that active galactic nuclei (AGN) of BL Lac type represent the most numerous extragalactic source type whereas pulsar wind nebulae (PWN) are the most common Galactic VHE emitters (see [Hinton & Hofmann 2009](#), for a review). H.E.S.S. has surveyed the region of the inner Galaxy to search systematically for VHE gamma-ray sources ([Aharonian et al. 2006](#)).

During a survey of the Galactic plane H.E.S.S. discovered the point-like source, HESS J1943+213 ([Abramowski et al. 2011](#)). At the position of the source counterparts (see Fig. 1) in the X-ray (IGR J19443+2117, CXOU J194356.2+211823, SWIFT J1943.5+2120), near-infrared (2MASS J19435624+2118233) and radio regime (NVSS J194356+211826) have been found (see [Abramowski et al. 2011](#)) but the nature of this source is still being debated. Based on the spectral energy distribution (SED) and on the assumption that those counterparts are associated with the VHE source, [Abramowski et al. \(2011\)](#) interpret this source as an extreme BL Lac shining through the Galactic plane. In contrast to that, [Gabányi et al. \(2013\)](#) found with VLBI observations

that the brightness temperature of the radio counterpart is substantially lower than expected from a relativistically beamed BL Lac jet and therefore argue that the object is a young PWN. [Leahy & Tian \(2012\)](#) conclude from a HI absorption measurement that this object is located at a distance of > 16 kpc, which is beyond the edge of the Galactic disk in this direction, and is thus of extragalactic origin. X-ray observations led with *Suzaku* ([Tanaka et al. 2014](#)) did not reveal any variability, which would have been a smoking gun for an extragalactic origin.

The prospective near-infrared counterpart to HESS J1943+213, namely 2MASS J19435624+2118233, offers a possibility to distinguish between these different interpretations and, for the purpose of this paper, we assume that 2MASS J19435624+2118233 is physically connected to the VHE gamma-ray source. The examination of the near-infrared counterpart is complicated by the bright Galactic dust emission at such low Galactic latitudes ($b = 1.29^\circ$). For an extragalactic scenario, the host galaxy of the BL Lac typically would be a giant elliptical galaxy (see, e.g., [Shaw et al. 2013](#)). Since the mean free path for VHE gamma rays from extragalactic sources is limited by attenuation on the extragalactic background light (EBL, see [Abramowski et al. 2013a](#)), any source of such highly energetic radiation should be located in the fairly local Universe ($z \lesssim 0.6$). In case the object

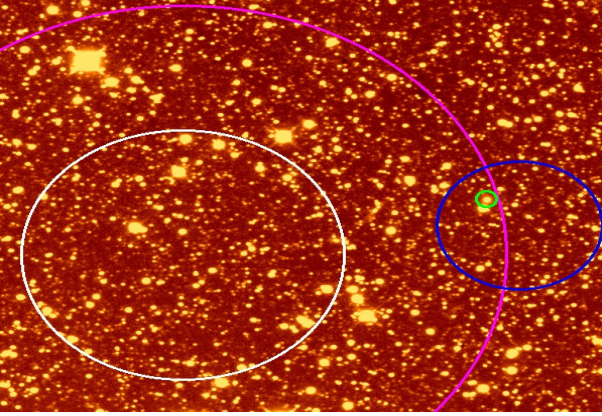


Fig. 1. 2MASS J19435624+2118233 and the VLBI, *Chandra* CXOU J194356.2+211823, HESS J1943+213, and *Fermi* objects. The 2MASS J19435624+2118233, VLBI and *Chandra* objects lie within the green circle. The blue circle denotes the error (1σ) circle of the H.E.S.S. observation, the white circle is the (1σ) statistical error circle of the *Fermi*-LAT observation, and the pink circle marks the (2σ) circle of the *Fermi*-LAT observation.

is a blazar, near-infrared imaging with longer integration times than what is provided by 2MASS (Two Micron All Sky Survey, Cutri et al. 2003) would resolve the giant elliptical host galaxy and show an extended, smooth, centrally concentrated light profile. In addition to the point-like, non-thermal infrared radiation from the AGN itself (e.g., Chen et al. 2005; Massaro et al. 2011), the host galaxy should emit extended thermal radiation from the stellar population, and absorption lines in the thermal spectra would allow a redshift measurement. For the PWN hypothesis a non-thermal spectrum would be expected throughout the whole nebula (e.g., Woltjer 1958; Zharikov et al. 2013), with a faint, diffuse near-infrared counterpart without a clearly defined center (e.g., Trimble 1968; Fesen et al. 2008). To conclude, imaging and spectral observations in the infrared can help to resolve the controversy over the nature of HESS J1943+213.

In addition to examining the near-infrared counterpart, exploring any high energy (HE, $100 \text{ MeV} < E < 100 \text{ GeV}$) counterpart will also lead to important constraints on the nature and distance of the VHE emitter. The currently operating Large Area Telescope (LAT) onboard the *Fermi* satellite provides deep observations of HESS J1943+213 in this energy range. Since VHE emission of distant extragalactic objects is attenuated by EBL whereas the HE radiation is much less affected by this attenuation, the connection of the HE and VHE spectrum can give evidence of an extragalactic origin of a gamma-ray emitter (Abdo et al. 2010; Sanchez et al. 2013).

This paper is structured in the following way. In Sect. 2 all infrared sources within the positional error circle of HESS J1943+213 are investigated, in Sect. 3 deep K -band observations of the most likely infrared counterpart are presented, in Sect. 4 the results of the LAT data analysis are given and in Sect. 5 constraints on the distance to the object and SED modeling of the gamma-ray source are discussed. Throughout this paper a Λ CDM cosmology with $H_0 = 71 \text{ km s}^{-1} \text{ Mpc}^{-1}$, $\Omega_\Lambda = 0.73$, and $\Omega_M = 0.27$ is assumed.

2. Infrared sources inside the error circle of the VHE gamma-ray source

In this section, color-color diagrams are used to check whether the properties of the prospective infrared counterpart

to HESS J1943+213, namely 2MASS J19435624+2118233, are consistent with other sources in the vicinity or if it represents an outlier with respect to the general properties of infrared sources there. The spectra of extragalactic sources are affected by the absorption by interstellar dust and are expected to be redder than foreground objects. Furthermore, non-thermal sources may occupy different regions in color-color diagrams with respect to thermal sources. The data for this investigation were retrieved from CDS Strasbourg through the Aladin tool (Bonnarel et al. 2000) and further processed with TOPCAT (Taylor 2005). The region around HESS J1943+213 was observed by the 2MASS, the UKIDSS (UKIRT Infrared Deep Sky Survey, Warren et al. 2007), and the WISE (Wide Field Infrared Survey Explorer, Wright et al. 2010) surveys. 2MASS J19435624+2118233 was detected by each of the surveys. 2MASS detects it only in the K -band and gives upper limits for J and H , while UKIDSS gives detections in J , H and K . Therefore, we took only the UKIDSS data of 2MASS J19435624+2118233 for further evaluation. The UKIDSS catalogue entries of 2MASS J19435624+2118233 are as follows: $\alpha_{J2000} = 19^{\text{h}}43^{\text{m}}56.24^{\text{s}}$, $\delta_{J2000} = 21^{\circ}18'23.3''$, ID J194356.23+211823.3, $J = 16.448 \pm 0.010 \text{ mag}$, $H = 15.187 \pm 0.006 \text{ mag}$, $K = 14.174 \pm 0.006 \text{ mag}$, and based on its spatial extent it has been classified as a galaxy with a 10% probability of being a star.

All objects within a radius of $1.5'$ around the source coordinate, $\alpha_{J2000} = 19^{\text{h}}43^{\text{m}}56.23^{\text{s}}$, $\delta_{J2000} = 21^{\circ}18'23.3''$, were used to construct a color-color diagrams. The radius of the region was chosen to coincide with the 99% positional confidence level of the H.E.S.S. source as shown in Abramowski et al. (2011).

Figure 2 shows the J - H - K diagram for all the objects retrieved from the database. The 2MASS and UKIDSS data show a concordant main distribution. The proposed infrared counterpart to HESS J1943+213 is outside of the main concentration of sources. The object is redder than most sources in $H - K$ as well as in $J - H$. The data points were not corrected for extinction by dust in the Galactic disk since the positions of the sources inside the Galaxy and thus actual extinctions are in most cases not known. Even after applying the extinction correction only for the counterpart of HESS J1943+213 (for extragalactic objects outside the Galactic disk the entire Galactic extinction applies) the object still remains off the main distribution.

To quantify the probability that the HESS J1943+213 belongs to the general distribution of objects in the error circle of $1.5'$ of the H.E.S.S. telescope we constructed a two-dimensional histogram of the UKIDSS color-color data. A Gaussian fit was applied to the histogram. This Gaussian is tilted by $\phi = -24$ degrees with respect to the axis of the color-color diagram. It has a minor axis standard deviation of $\sigma_1 = 0.09 \text{ mag}$ and a major axis standard deviation of $\sigma_2 = 0.16 \text{ mag}$. The distance between HESS J1943+213 and the center of the Gaussian is 7.8σ with

$$\sigma = \left| \begin{pmatrix} \cos(\phi) & \sin(\phi) \\ -\sin(\phi) & \cos(\phi) \end{pmatrix} \begin{pmatrix} \sigma_1 \\ \sigma_2 \end{pmatrix} \right|. \quad (1)$$

As the extinction is not well known in this region of the Galaxy we checked the closest distance between a line through the position of HESS J1943+213 and the extinction direction (A_V arrow; extinction correction follows Schlafly & Finkbeiner 2011, i.e. $A_J = 1.952 \text{ mag}$, $A_H = 1.936 \text{ mag}$, $A_K = 0.832 \text{ mag}$ in the color-color diagram. This closest distance is still 2.4σ . This position is reached for a differential extinction between the main distribution and HESS J1943+213 of about 10 mag .

The parameters of the Gaussian fit are the same within 5% for histograms with different binnings, and there are minor

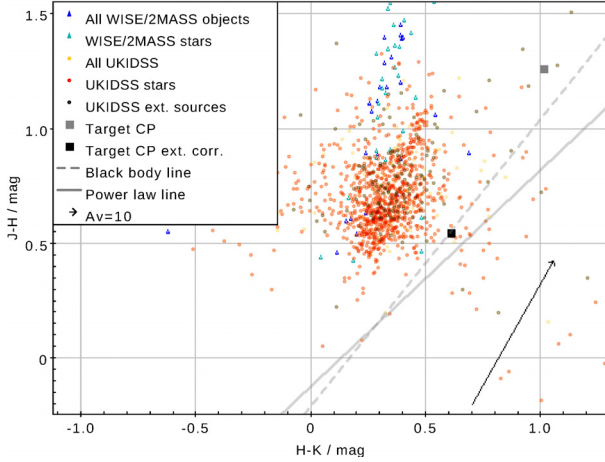


Fig. 2. Color-color plot in the J , H and K bands for the infrared sources within the error circle of HESS J1943+213. The infrared counterpart 2MASS J19435624+2118233 is clearly redder than the main distribution of sources in this direction of the sky. The arrow indicates the direction of reddening by extinction by interstellar dust for $A_V = 10$.

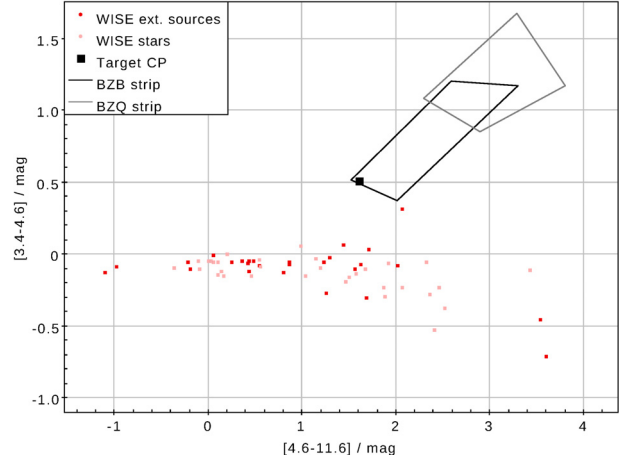


Fig. 3. Color-color plot in the WISE W1, W2 and W3 bands for the infrared sources within the HESS J1943+213 error circle. 2MASS J19435624+2118233 is located within the so-called “Blazar strip”. No correction for extinction on interstellar dust has been applied. Note that BZB stand for BL Lac objects while BZQ for flat-spectrum radio quasars.

changes to the analysis above if one only uses the distribution of stars only instead of the distribution of all objects.

Figure 2 shows also the black body line (for redshift $z = 0$) and the power-law lines, which were taken from Chen et al. (2006). These lines were obtained with the measured value for the Mauna Kea Observatories Near-Infrared Filter Set (Tokunaga & Vacca 2005), which are used for the UKIDSS survey ($J = 1.25 \mu\text{m}$, $H = 1.644 \mu\text{m}$, $K_s = 2.198 \mu\text{m}$, $S_J = 1560 \text{ Jy}$, $S_H = 1040 \text{ Jy}$, $S_K = 645 \text{ Jy}$). The extinction corrected measurement of 2MASS J19435624+2118233 falls on the black body line, which would lead to the conclusion that the object is thermally dominated¹ in the near-infrared. However, due to the large and potentially uncertain extinction, this conclusion has to be taken with caution.

In a second step we studied the mid-infrared measurements of the WISE survey. WISE observed the sky in four mid-infrared bands: $W1 = 3.4 \mu\text{m}$, $W2 = 4.6 \mu\text{m}$, $W3 = 12 \mu\text{m}$, and $W4 = 22 \mu\text{m}$. The AllWISE catalogue entry for the counterpart to 2MASS J19435624+2118233 is: ID J194356.24+211822.9, position: $\alpha_{J2000} = 19^{\text{h}}43^{\text{m}}56.24^{\text{s}}$, $\delta_{J2000} = 21^{\circ}18'23.3''$, $W1 = 13.056 \pm 0.116 \text{ mag}$, $W2 = 12.523 \pm 0.094 \text{ mag}$, $W3 = 10.909 \pm 0.180 \text{ mag}$, $W4 > 8.144 \text{ mag}$. In Fig. 3 the $[3.4]-[4.6]-[12] \mu\text{m}$ color-color diagram is shown. No correction for extinction on interstellar dust has been applied. However, it has to be noted that mid-infrared radiation is only mildly affected by dust extinction. The empirically found blazar strips of Massaro et al. (2011) are also drawn in this diagram. These strips represent the area in this color-color diagram where blazars lie. This is interpreted as due to their mid-infrared colors being consistent with non-thermal radiation. 2MASS J19435624+2118233 is clearly located at the edge of the Blazar strip in the mid-infrared, indicating that the emission in this energy band is dominated by non-thermal emission.

To summarize, 2MASS J19435624+2118233 appears to be of extragalactic origin and can likely be classified as a blazar.

3. CAHA observations

On July, 25 and 26, 2013 we observed the region around HESS J1943+213 with the wide field camera OMEGA2000

¹ This thermal emission is related to the host galaxy, see Sect. 5.

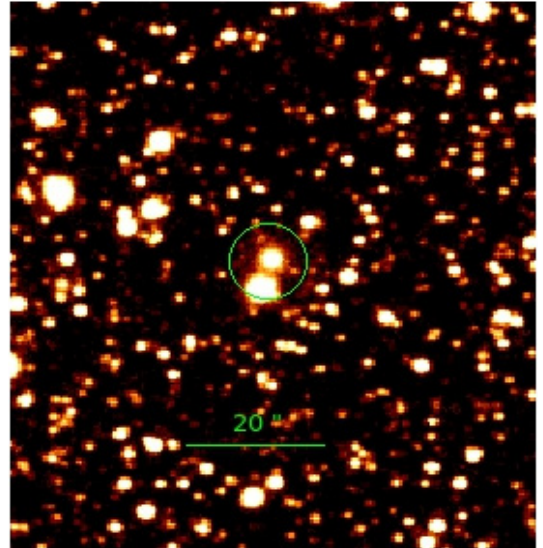


Fig. 4. The object and its neighbourhood. The green circle is centered on the target. The object in the lower part of the circle is one of the stars ($\alpha_{J2000} = 19^{\text{h}}44^{\text{m}}00.0^{\text{s}}$, $\delta_{J2000} = 21^{\circ}17'16.1''$) used to determine the target coordinates.

installed on the 3.5 m telescope at Calar Alto (Kovács et al. 2004) of the Centro Astronomico Hispano Aleman. On July, 25 we used the K -short filter and on July, 26 K -prime. The field was centered on the X-ray counterpart of the object. The target was observed 30 min in total each night. For sky subtraction we took separate sky frames as the object is in the Galactic plane. The seeing was $1.1''$ on the first and $1.6''$ on the second night with poor transparency during both nights.

Figure 4 shows the near-infrared counterpart and its neighborhood. The position of the object was determined using 8 bright stars of the 2MASS catalogue within a circle of $3'$ radius. The coordinate system data were scaled and rotated using the 28 connecting lines between these stars. The position of 2MASS J19435624+2118233 was determined to be $\alpha_{J2000} = 19^{\text{h}}43^{\text{m}}56.3^{\text{s}} \pm 0.1^{\text{s}}$, $\delta_{J2000} = 21^{\circ}18'23.4'' \pm 0.2''$ which agrees with the VLBI position to better than $0.1''$ (Gabányi et al. 2013).

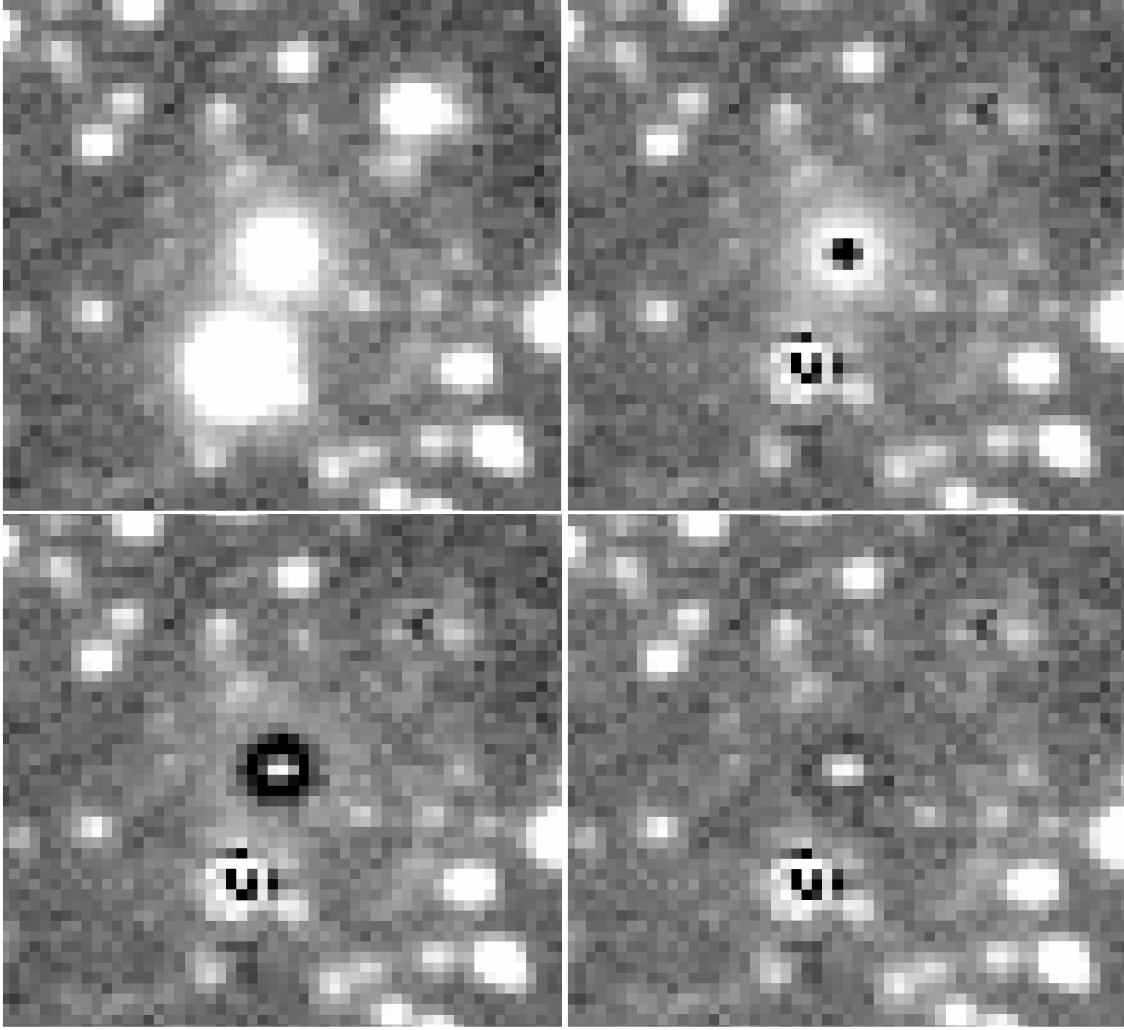


Fig. 5. *K*-band image of the infrared counterpart of HESS J1943+213 ($25'' \times 25''$). The image at the top left is centered on 2MASS J19435624+2118233, the prospective infrared counterpart of the VHE gamma-ray source. The next 3 panels show residuals after subtracting, at the top right, a point source, at the bottom row from left to right, an exponential surface brightness profile, and a surface brightness profile with Sérsic index 7. The package `galfit` was used to determine the best-fitting free parameters (magnitude and, for the extended profiles, half-light radius). Bright, neighboring stars were also subtracted to avoid confusion. The prominent residual after subtracting a point source clearly demonstrates that the infrared counterpart to HESS J1943+213 is extended (to be compared with the residual from the bright star directly below HESS J1943+213). Furthermore, a high-Sérsic index profile leaves a smaller residual than an exponential profile, indicating that the surface brightness profile of HESS J1943+213 follows that of a typical, massive elliptical galaxy more closely than that of a disk galaxy. The moderate residual for the high-Sérsic index model hints at the presence of a central point source, but imaging with higher resolution is needed to confirm this.

The flux of the object was determined to be $13.5 \text{ mag} \pm 0.3 \text{ mag}$ in *K*. The higher brightness with respect to the UKIDSS measurement results from faint outer regions of the extended source that were missed by the shallower UKIDSS image. We checked the variation of the flux between single exposures and night 1 and night 2. The maximum variation in the flux was measured to be 0.5 mag, which is of the level of measured flux variations due to sub pixel shifts of the object. Thus no variability in the timespan of 30 min and between night 1 and night 2 was detected.

To classify the object and its morphology we used two different approaches. With the first approach we used `galfit` (Peng et al. 2010). The object was modeled with a Sérsic profile (Sérsic 1963):

$$I[r] = I_e \exp(-a(r/r_e)^{1/n} - 1) \quad (2)$$

with $I[r]$ the intensity at radius r , $I_e = I[0]/e$, a a normalization factor, r_e the half light radius, and n the Sérsic parameter.

Due to the number of sources in the field we could not let the program find the Sérsic index and half light radius automatically but had to rerun the program for different values of these parameters to find the best fit. In Fig. 5 the morphology of the source is investigated. Subtracting a point-like source clearly leaves residuals, thus showing that the object is extended. These residuals are significant at the 50σ confidence level when compared to background fluctuations in blank fields of the sky. In order to determine if the object could be a disk galaxy or an elliptical we made a best-fit approach with an exponential profile and Sérsic index profiles with different indices. We found that a high-Sérsic index profile leaves a smaller residual than an exponential profile, indicating that the surface brightness profile of HESS J1943+213 follows that of a typical, massive elliptical galaxy more closely than that of a disk galaxy. The object is round (axis ratio >0.97) and has a half light radius of $\approx 2.0'' < r_e < 2.5''$. The Sérsic index n for the best fit with `galfit` was determined to be 8.

We double checked the results with a custom algorithm in IDL. The program was used to fit a point-spread function (PSF) taken from the image of a neighboring star and a Sérsic profile convolved with the PSF to the data. Here we left the positions and half light radius free to vary but fixed the Sérsic parameter. For the PSF fitting we used different stars. The alternative method also yielded a half light radius of $\approx 2.0'' < r_e < 2.5''$. The Sérsic index n for the best fit was determined to be > 7 . Therefore, the results from the two methods are consistent. A moderate residual for the high-Sérsic index model suggests the presence of a central point source. Higher-resolution imaging will be needed to confirm this feature.

To summarize, 2MASS J19435624+2118233 appears to be an elliptical galaxy and can likely be classified as a blazar. Given the correspondence of the position between 2MASS J19435624+2118233 and the VLBI and *Chandra* object it can be assumed that it is the same object. Given this multi-wavelength property of the object we conclude that 2MASS J19435624+2118233 is a viable counterpart to HESS J1943+213.

4. *Fermi*-LAT observations

The LAT is sensitive to gamma rays from 20 MeV to > 300 GeV. A detailed description of the instrument and its performance is given in [Atwood et al. \(2009\)](#). The LAT mainly operates in survey mode in which the entire sky is observed every three hours.

For the analysis of the LAT data, the events belonging to the class SOURCE ([Ackermann et al. 2012](#)) have been retained. Considering that the object is located in the Galactic plane, the energy range has been restricted to 1–300 GeV. This cut reduces the diffuse Galactic background which presents a rather soft spectrum compared to a hypothetical LAT counterpart of a TeV blazar. A region of interest of 10° radius around the coordinates of HESS J1943+213 was defined to perform a binned analysis ([Mattox et al. 1996](#)), implemented in the `gtlike` tool, part of the ScienceTools² V9R32P5. Cuts were applied on the rocking angle of the spacecraft, which was required to be smaller than 52° , and on the zenith angle of the events, required to be smaller than 100° to reduce Earth limb gamma-rays. The Pass 7 Reprocessed data ([Bregeon et al. 2013](#)), from August, 4 2008 to August, 4 2013, were used in this study together with the corresponding instrument response functions P7REP_SOURCE_V15. The last Galactic diffuse model (`gll_iem_v05_rev1.fit`) and the public isotropic model (`iso_source_v05.txt`) were included in the sky model³ as well as all the sources within 15° around HESS J1943+213 present in a preliminary list of sources, currently only available to the LAT Collaboration, based on 4 years of data (3FGL). Sources within 3° of the target have their spectral parameters free to vary during the optimization procedure and the other parameters are frozen to the best fit values of the 4 year list. Finally a source, with a power-law spectrum, was added to the sky model at the position of HESS J1943+213. After an initial fit, the sources with Test Statistic⁴ lower than 1 were removed and the fitting procedure was redone.

² <http://fermi.gsfc.nasa.gov/ssc/data/analysis/software/>

³ Files are available at <http://fermi.gsfc.nasa.gov/ssc/data/access/lat/BackgroundModels.html>

⁴ See http://fermi.gsfc.nasa.gov/ssc/data/analysis/documentation/Cicerone/Cicerone_Likelihood/Likelihood_overview.html for a definition.

A counterpart to HESS J1943+213 is detected above 1 GeV. To better locate the GeV counterpart, the tool `gtfindsrc` has been used yielding a position $\alpha_{J2000} = 19^{\text{h}}44^{\text{m}}05^{\text{s}}$, $\delta_{J2000} = 21^\circ 17' 51''$ with a 1σ error circle radius of $1' 12''$ (error is statistical only), at an angular separation of $2' 24''$ from the position of HESS J1943+213. At this location, the counterpart is detected above 1 GeV at a TS of 36.0 (corresponding to $\approx 5.1\sigma$ for 4 degrees of freedom⁵). Taken the LAT systematical uncertainties ([Nolan et al. 2012](#)) and H.E.S.S. uncertainties⁶, the positions are marginally in agreement (below 2σ). The good agreement of the HE and VHE spectra (see later and Fig. 7) also favor a common origin of the measured emission.

Using the LAT position, the resulting best-fit spectrum is a power law with a normalization of $(3.0 \pm 0.8_{\text{stat}} \pm 0.6_{\text{sys}}) \times 10^{-15} \text{ cm}^{-2} \text{ s}^{-1} \text{ MeV}^{-1}$ at the decorrelation energy $E_{\text{dec}} = 15.1$ GeV and a spectral index of $\Gamma = 1.59 \pm 0.19_{\text{stat}} \pm 0.13_{\text{sys}}$ yielding an integral flux between 1 GeV and 300 GeV of $I = (3.7 \pm 1.3_{\text{stat}} \pm 0.8_{\text{sys}}) \times 10^{-10} \text{ cm}^{-2} \text{ s}^{-1}$. The highest energy photon that can be associated with the counterpart (with a probability higher than 80%) has $E = 51$ GeV. Systematic uncertainties from the modeling of the LAT effective area were evaluated using the IRF bracketing method ([Abdo et al. 2009](#)) and by using alternative interstellar emission models ([de Palma et al. 2013](#)) for the Galactic diffuse model. Data points were obtained by repeating the analysis in restricted energy ranges equally spaced in log energy. No variability has been found for this source using an unbinned Bayesian block analysis ([Scargle et al. 2013](#)). Note that, since this source is in the Galactic plane, the modeling of the Galactic diffuse emission might have a significant impact on the spectral parameters which has been evaluated and taken into account in the systematical uncertainties. [Tanaka et al. \(2014\)](#) did not find a significant detection of the source above 10 GeV using 4.5 years of Pass 7 data. They reported a low-significance spectral measurement in the range 10–300 GeV with an index of $\Gamma \approx 2.4$. Repeating the analysis described here in the same energy range leads to an index of $\Gamma = 2.26^{+0.53}_{-0.47}$. This can be interpreted as the sign of a rollover of the photon spectrum and is in agreement with the softer VHE measurement of H.E.S.S.

5. Discussion

5.1. Host galaxy and redshift

In this paper we have studied 2MASS J19435624+2118233, which we assume to be the infrared counterpart of HESS J1943+213 and additionally, we have detected the source in HE gamma-rays with the LAT. These observations place important constraints on the nature of the object. We investigated all infrared sources within the error circle of HESS J1943+213 and found that 2MASS J19435624+2118233 is redder than the bulk of infrared sources at this location on the sky and that it falls in the blazar strip ([Massaro et al. 2011](#)) in the mid-infrared. Using the 3.5 m CAHA telescope we found that the *K*-band counterpart 2MASS J19435624+2118233 is extended. These observational results strongly suggest that 2MASS J19435624+2118233 is of extragalactic origin. The extended counterpart of the 2MASS source represents the host galaxy of a BL Lac type object and is a viable counterpart to HESS J1943+213. The extension of the object can even give

⁵ The degrees of freedom are two spectral parameters and the position (two parameters).

⁶ The best position reported is $\alpha_{J2000} = 19^{\text{h}}43^{\text{m}}55^{\text{s}} \pm 1^{\text{s}}_{\text{stat}} \pm 1^{\text{s}}_{\text{sys}}$, $\delta_{J2000} = +21^\circ 18' 8'' \pm 17''_{\text{stat}} \pm 20''_{\text{sys}}$.

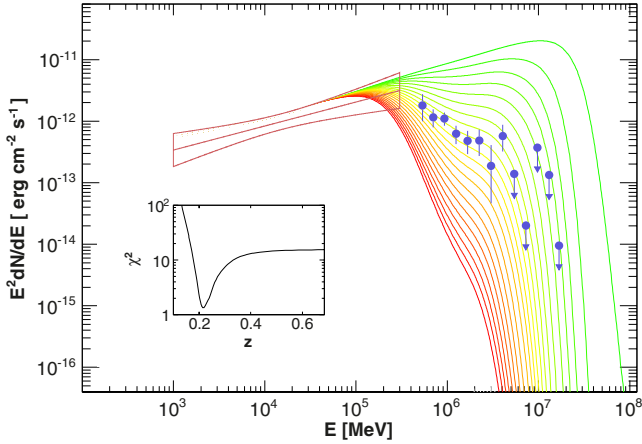


Fig. 6. Spectral energy distribution of HESS J1943+213 in γ -rays. The *Fermi*-LAT error contour (red) has been extrapolated toward the H.E.S.S. energy range (blue points) and corrected for EBL absorption using the model of Franceschini et al. (2008) assuming different values for z from $z = 0.01$ (green line) to $z = 0.7$ (red line). The inset gives the corresponding χ^2 as a function of the redshift z .

constraints on the distance to the host galaxy. BL Lac host galaxies typically have infrared half radii of 3.1 ± 1.7 kpc (Cheung et al. 2003)⁷. For the measured half light radius of 2MASS J19435624+2118233 of $2.5''$ this would correspond to an angular diameter distance D_A and redshift z of $D_A = 120$ Mpc ($z \approx 0.03$) for a half light radius of 1.4 kpc, $D_A = 260$ Mpc ($z \approx 0.07$) for a half light radius of 3.1 kpc and $D_A = 410$ Mpc ($z \approx 0.11$) for a half light radius of 4.8 kpc (Wright et al. 2006). Since the half-light radius of the BL Lac host is not very well defined, this places only loose constraints on the distance and redshift of the object. The lower limit adopted in this work is $z > 0.03$. For comparison, using the typical K -band luminosity of BL Lac host galaxies Abramowski et al. (2011) found a redshift of $z \gtrsim 0.14$.

A constraining upper limit on the redshift can be obtained by comparing the H.E.S.S. data points with the *Fermi*-LAT results, extrapolated to the TeV energies and corrected for EBL absorption assuming different values for z . The model of EBL used in this work is described in Franceschini et al. (2008). For each extrapolation, a χ^2 is then computed to estimate the most likely value of z (Abdo et al. 2010). To be conservative, the error on differential flux computed using Eq. (2) of Abdo et al. (2010) was added to the differential flux. Figure 6 gives the results for different values of z as well as the evolution of the χ^2 as a function of the redshift. A minimum is reached for $z \approx 0.22$. An upper limit at 0.45 can be set with a confidence level of 95%.

Another method was proposed by Sanchez et al. (2013) to roughly estimate the redshift based on the spectral break between the GeV and TeV energy ranges. Applying this method leads to an upper limit of $z < 0.39$, which provides a cross-check with the previous method. Summarizing, if HESS J1943+213 is assumed to be 2MASS J19435624+2118233 our findings limit its redshift to be between 0.03 and 0.45.

5.2. SED modeling

Blazars present a double humped SED with a low-energy (from radio to X-ray) peak attributed to synchrotron emission of relativistic electrons. The origin of the HE component is still

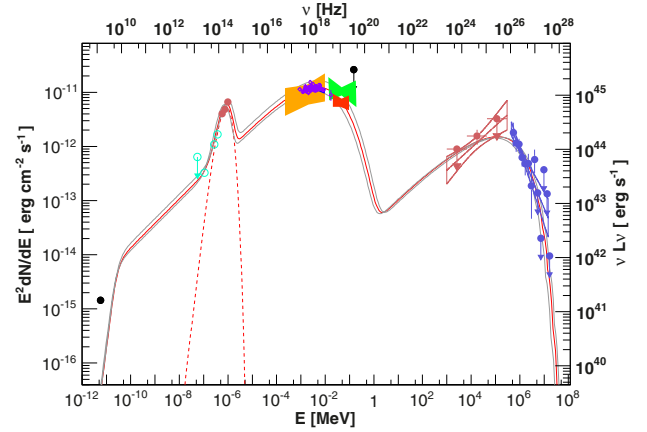


Fig. 7. Spectral energy distribution of HESS J1943+213. Empty blue circles are the WISE data and the red circles the CAHA results. The red butterfly is the *Fermi*-LAT best-fit power law and the 68% error contour. A 2σ upper limit is reported for the LAT data points if $TS < 9$. Other data were extracted from Abramowski et al. (2011): the black point is the NVSS measurement, the yellow, blue, and red butterflies are respectively the *Chandra*, *Swift*-XRT, and INTEGRAL-IBIS measurements. The green point is from the 70-month *Swift*-BAT catalogue (Baumgartner et al. 2013). The upper limit is from INTEGRAL-SPI. The purple points are the *Suzaku* measurements extracted from Tanaka et al. (2014). The red line is the result of the SSC calculation for $z = 0.2$, and the grey lines were obtained for $z = 0.03$ and $z = 0.45$.

Table 1. Parameters values of the SSC model used to reproduce the SED of HESS J1943+213.

| Parameters | Value |
|-----------------------|----------------------|
| B [G] | 0.05 |
| R [cm] | 8.5×10^{16} |
| δ | 10 |
| p | 2.1 |
| γ_{cut} | 10^6 |
| N_{tot} | 4.7×10^{53} |

uncertain. The leptonic class of models invoke the production of gamma-rays by inverse Compton scattering on synchrotron photons (synchrotron self-Compton, SSC, Band & Grindlay 1985) or on an external field (external Compton, Dermer & Schlickeiser 1993).

An SSC model has been used to reproduce the SED of the source presented in Fig. 7. A single spherical emission zone of size R filled with a uniform magnetic field B has been considered. The emission zone is moving relativistically toward the Earth with a Doppler factor δ . The electron distribution, $N_e(\gamma)$, is described by a power law with an exponential cut-off of the form $N_e(\gamma) \propto \gamma^{-p} \cdot \exp(-\gamma/\gamma_{\text{cut}})$ from $\gamma_{\text{min}} = 1$ to $\gamma_{\text{max}} = 10^{10}$. A redshift of 0.2 has been assumed for the SSC calculation, which leads to a luminosity distance of $D_L = 971$ Mpc (Wright et al. 2006). The results of the SSC calculation and the black-body emission are shown in Fig. 7 and the parameters are given in Table 1. For completeness, the calculations for $z = 0.03$ and $z = 0.45$ are shown in Fig. 7.

The host galaxy is fitted using a black-body model (Katarzyński et al. 2003) assumed to originate from thermal emission, with a temperature of 3000 K and a total luminosity of 4.5×10^{44} erg s⁻¹. The near-infrared measurements rule out a pure power law for this energy regime. In this calculation, the jet is out of equipartition, the ratio between the kinetic energy of the electrons and the magnetic energy being $Q = u_e/u_B = 12$.

⁷ Scaled to the adopted cosmology.

Exhibiting a jet dominated by the energy of the electrons seems to be a feature of the TeV high-frequency peaked BL Lacs, see e.g. Mrk 421 (Abdo et al. 2011a), Mrk 501 (Abdo et al. 2011b), SHBL J001355.9–185406 (Abramowski et al. 2013b) or 1ES 1312–423 (Abramowski et al. 2013c).

6. Outlook

The nature of the VHE emitter HESS J1943+213 has been disputed in the past (Abramowski et al. 2011; Gabányi et al. 2013; Leahy & Tian 2012) with diverging conclusions whether the object is of Galactic or extragalactic origin. In this work we have found that the infrared and HE counterparts show a consistent picture that points toward an extreme blazar hosted by a giant elliptical galaxy. Additionally, the infrared surface brightness of the prospective host galaxy appears to be more centrally peaked than expected for a giant elliptical galaxy, thus indicating that a central point source may be present in this system. Further observations in radio and possibly infrared will be required to finally settle the unexplained properties of this enigmatic source.

Acknowledgements. D.S. work is partially supported by the LABEX grant enigmass. The authors want to thank T. Cheung for discussions on the host galaxies of BL Lac's and an anonymous referee for helpful comments. D.P., W.D. and W.G. want to thank the Pinte for its inspiring spirits and the EMBL cantine for the sustenance, which supported us during all this work. The *Fermi*-LAT Collaboration acknowledges generous ongoing support from a number of agencies and institutes that have supported both the development and the operation of the LAT as well as scientific data analysis. These include the National Aeronautics and Space Administration and the Department of Energy in the United States, the Commissariat à l'Énergie Atomique and the Centre National de la Recherche Scientifique/Institut National de Physique Nucléaire et de Physique des Particules in France, the Agenzia Spaziale Italiana and the Istituto Nazionale di Fisica Nucleare in Italy, the Ministry of Education, Culture, Sports, Science and Technology (MEXT), High Energy Accelerator Research Organization (KEK) and Japan Aerospace Exploration Agency (JAXA) in Japan, and the K. A. Wallenberg Foundation, the Swedish Research Council and the Swedish National Space Board in Sweden. Additional support for science analysis during the operations phase is gratefully acknowledged from the Istituto Nazionale di Astrofisica in Italy and the Centre National d'Études Spatiales in France.

References

- Abdo, A. A., Ackermann, M., Ajello, M., et al. (Fermi-LAT Collaboration) 2009, *ApJ*, 707, 1310
- Abdo, A. A., Ackermann, M., Ajello, M., et al. (Fermi-LAT Collaboration) 2010, *ApJ*, 708, 1310
- Abdo, A. A., Ackermann, M., Ajello, M., et al. (Fermi-LAT Collaboration) 2011a, *ApJ*, 736, 131
- Abdo, A. A., Ackermann, M., Ajello, M., et al. (Fermi-LAT Collaboration) 2011b, *ApJ*, 727, 129
- Abramowski, A., Acero, F., Aharonian, F., et al. (H.E.S.S. Collaboration) 2011, *A&A*, 529, A49
- Abramowski, A., Acero, F., Aharonian, F., et al. (H.E.S.S. Collaboration) 2013a, *A&A*, 550, A4
- Abramowski, A., Acero, F., Aharonian, F., et al. (H.E.S.S. Collaboration) 2013b, *A&A*, 554, A72
- Abramowski, A., Acero, F., Aharonian, F., et al. (H.E.S.S. Collaboration) 2013c, *MNRAS*, 434, 1889
- Ackermann, M., Ajello, M., Albert, A., et al. (Fermi-LAT Collaboration) 2012, *ApJS*, 203, 4
- Aharonian, F., Akhperjanian, A. G., Bazer-Bachi, A. R., et al. (H.E.S.S. Collaboration) 2006, *ApJ*, 636, 777
- Atwood, W. B., Abdo, A. A., Ackermann, M., et al. (Fermi-LAT Collaboration) 2009, *ApJ*, 697, 1071
- Band, D. L., & Grindlay, J. E. 1985, *ApJ*, 298, 128
- Baumgartner, W. H., Tueller, J., Markwardt, C. B., et al. 2013, *ApJS*, 207, 19
- Bonnarel, F., Fernique, P., Bienaymé, O., et al. 2000, *A&AS*, 143, 33
- Bregeson, J., Charles, E., Wood, M. for the Fermi-LAT Collaboration 2013, 2012 Fermi Symp. Proc., eConf C121028
- Chen, P. S., Fu, H. W., & Gao, Y. F. 2005, *New Astron.*, 11, 27
- Chen, P. S., Shan, H. G., & Gao, Y. F. 2006, *New Astron.*, 11, 557
- Cheung, C. C., Urry, C. M., Scarpa, R., & Giavalisco, M. 2003, *ApJ*, 599, 155
- Cutri, R. M., Skrutskie, M. F., van Dyk, S., et al. 2003, *VizieR On-line Data Catalog: II/246*, originally published in: University of Massachusetts and Infrared Processing and Analysis Center (IPAC/California Institute of Technology)
- Dermer, C. D., & Schlickeiser, R. 1993, *ApJ*, 416, 458
- de Palma, F., Brandt, T. J., Johannesson, G., Tibaldo, L. for the Fermi LAT Collaboration 2013, 2012 Fermi Symp. Proc., eConf C121028
- Fesen, R., Rudie, G., Hurford, A., et al. 2008, *ApJS*, 174, 379
- Franceschini, A., Rodighiero, G., & Vaccari, M. 2008, *A&A*, 487, 837
- Gabányi, K. É., Dubner, G., Giacani, E., et al. 2013, *ApJ*, 762, 63
- Hinton, J. A., & Hofmann, W. 2009, *ARA&A*, 47, 523
- Katarzyński, K., Sol, H., & Kus, A. 2003, *A&A*, 410, 101
- Kovács, Z., Mall, U., Bizenberger, P., Baumeister, H., & Röser, H.-J. 2004, *SPIE*, 5499, 432
- Leahy, D. A., & Tian, W. W. 2012, *A&A*, 539, A128
- Massaro, F., D'Abrusco, R., Ajello, M., et al. 2011, *ApJ*, 740, L48
- Mattox, J. R., Bertsch, D. L., Chiang, J., et al. 1996, *ApJ*, 461, 396
- Nolan, P. L., Abdo, A. A., Ackermann, M., et al. 2012, *ApJS*, 199, 31
- Peng, C. Y., Ho, L. C., Impey, C. D., & Rix, H.-W. 2010, *AJ*, 139, 2097
- Sanchez, D. A., Fegan, S., & Giebels, B. 2013, *A&A*, 554, A75
- Scargle, J. D., Norris, J. P., Jackson, B., & Chiang, J. 2013, 764, 167
- Schlaflly, E. F., & Finkbeiner, D. P. 2011, *ApJ*, 737, 103
- Sérsic, J. L. 1963, *BAAA*, 6, 41
- Shaw, M. S., Romani, R. W., Cotter, G., et al. 2013, *ApJ*, 764, 135
- Taylor, M. B. 2005, *ASPC*, 347, 29
- Tanaka, Y. T., Stawarz, L., Finke, J., et al. 2014, *ApJ*, 787, 155
- Tokunaga, A. T., & Vacca, W. D. 2005, *PASP*, 117, 421
- Trimble, V. 1968, *AJ*, 73, 535
- Warren, S. J., Hambly, N. C., Dye, S., et al. 2007, *MNRAS*, 375, 213
- Woltjer, L. 1958, *BAN*, 14, 39
- Wright, E. L. 2006, *PASP*, 118, 1711
- Wright, E. L., Eisenhardt, P. R. M., Mainzer, A. K., et al. 2010, *AJ*, 140, 1868
- Zharikov, S. V., Zyuzin, D. A., Shibanov, Y. A., & Mennickent, R. E. 2013, *A&A*, 554, A120